

Near-field scanning optical microscope probe analysis

Petr Klapetek^{a,*}, Jiří Buršík^b, Miroslav Valtr^a, Jan Martinek^c

^a*Czech Metrology Institute, Okružní 31, 638 00 Brno, Czech Republic*

^b*Institute of Physics of Materials, Žitkova 22, 616 62 Brno, Czech Republic*

^c*Brno University of Technology, Žitkova 17, 602 00 Brno, Czech Republic*

Received 23 April 2007; received in revised form 8 September 2007; accepted 26 October 2007

Abstract

In this article results of a comparison of two NSOM probe characterization methods are presented. Scanning electron microscopy analysis combined with electromagnetic field modeling using the finite difference in time domain method are compared with measured far-field radiation diagrams of NSOM probes. It is shown that measurement of far-field radiation diagrams can be an efficient tool for daily checking of the NSOM probes quality. Moreover, it is shown that the inner probe geometry has large influence on the directional radiation of an NSOM probe and the far-field radiation diagram can be used as a simple method to distinguish between different probe geometries.

© 2007 Elsevier B.V. All rights reserved.

PACS: 68.37.Uv; 78.68.+m

Keywords: NSOM; Artifacts

1. Introduction

Near-field scanning optical microscopy (NSOM) is a technique belonging to the family of scanning probe microscopy instruments. Within the NSOM instrument the microscope probe is formed by a nanometer-scale light source (or light detector) that is scanning over the surface, usually in the constant gap mode [1,2].

Near-field optical microscope is often referred to as an instrument being capable of producing optical images (e.g. reflection or transmission) comparable to the classical microscopy, but having much better resolution. However, quantitative analysis of optical images obtained using NSOM technique is not usually performed as there are too many issues unclear from the experimental point of view. First of all, the exact shape of an NSOM probe (including its aperture) is not known and cannot be easily determined during the measurement. Moreover, the electromagnetic field distribution within the probe and in the near-field

region and the probe's inner geometry are also unknown. Finally, topographical artifacts that arise from varying the near-field electromagnetic distribution over rapidly changing sample topography are very often observed.

One of the largest problems in interpretation or further quantitative analysis of optical data obtained by means of NSOM is its relation to the local surface topography [3–5,12–14]. This effect can be easily seen while imaging steep slopes or edges on the sample (here, it can be easily predicted) or while imaging surface exhibiting random roughness. Sometimes topography artifacts can modify or even completely obscure the optical information contained in the data, namely due to the fact that the variations of the sample refractive index and topographic variations can lead to the same effects on the NSOM data [6].

For all the methods of evaluating the probe-sample artifacts the probe geometry must be determined first. In this article, two probe geometry analysis methods are compared. First, the probes are analyzed by scanning electron microscopy (e.g. see Fig. 1). Second, their far-field radiation diagrams are measured [7,8]. Finally, the experimental results are compared with help of the finite

*Corresponding author. Tel.: +420 54555337; fax: +420 54555183.
E-mail address: klapetek@physics.muni.cz (P. Klapetek).

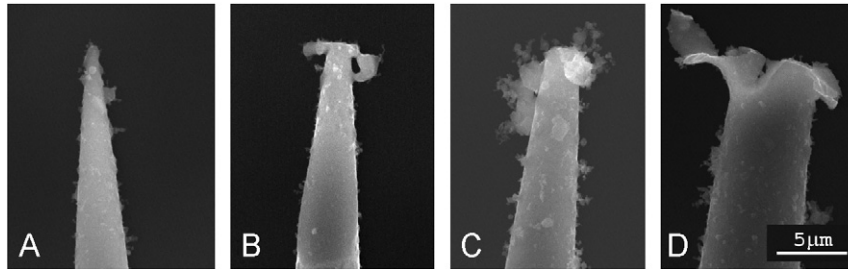


Fig. 1. Scanning electron microscopy images of four different NSOM aperture probes. The magnification is same for all the images.

difference in time domain (FDTD) method modeling of far-field radiation diagrams. Analyzed probes are used for NSOM measurements on standard samples to prove their real resolution.

2. NSOM probe geometry analysis

2.1. Experimental NSOM probe geometry measurement

For an estimation of the NSOM probe geometry we can use three methods generally used in atomic force microscopy:

- Scanning over known structures—imaging the tip directly using a tip characterization sample containing known topographical structures much sharper than the tip itself.
- Blind tip estimation—using random roughness or other topographic features on measured sample together with blind tip estimation algorithm [10].
- Scanning electron microscopy—imaging the NSOM tip in a scanning electron microscope before or after measurement.

Even if the methods mentioned here are used regularly for atomic force microscopy tip shape determination, they are not very suitable for NSOM probe analysis. As the NSOM probe is usually much more susceptible to destruction while scanning at non-optimal conditions, the methods based on special topographic features (that are usually very sharp) can lead to tip changes very easily. Scanning electron microscopy is therefore the only really non-destructive method for analysis of NSOM probes geometry.

Using all the above-mentioned methods we can analyze the outer probe geometry. However, we still do not have information about the inner geometry—i.e. about the material distribution within the probe. As the probe consists of at least three different materials—a transparent core, transparent cladding and metal shielding—it can be assumed that the effect of distribution of these materials within the probe affects the NSOM images highly. This effect will be studied numerically in the next section.

For a simple analysis of these effects we have developed a simple method based on the measurement of far-field probe radiation diagrams (see Fig. 2). In contrast to

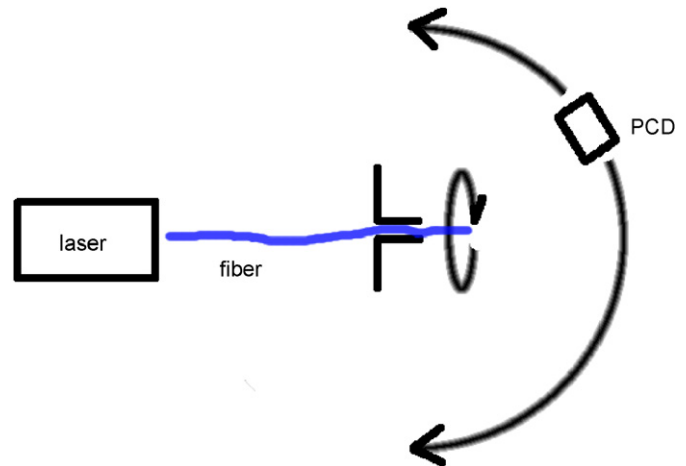


Fig. 2. Geometry used for the far-field radiation measurements.

Ref. [7] the method used in this article is two-dimensional in order to detect radiation into all the directions, as the radiation diagrams coming from heavily corrupted probes are highly anisotropic. Various defects appearing on the probe apex that are responsible for electromagnetic field scattering in the near-field region lead to a change in the probe radiation in the far-field region as well [11]. Therefore, we can expect that we can use the far-field data to reconstruct partly the complete information about both the inner and the outer probe geometry that is present only in the near-field region. To model this effect we have used the FDTD method as described in the next section.

2.2. NSOM probe modeling

There are several methods found in the literature that can be used for modeling the electromagnetic field within the probe-sample region in NSOM. First of all, a simple geometric approach based on the tip-sample dilation algorithm and dipole source radiation can be used for a simplified geometry [12]. This method can be efficient in predicting the main topographic artifacts; however, for any quantitative analysis it can be considered to be over-simplified. More sophisticated methods used for NSOM geometries include direct moment method [15], Green's tensor technique [6] and reciprocal-space perturbative

method [9]. All these methods allow us to model relatively complicated geometries, thus simulating real signals in NSOM.

Finally, a time stepping finite element method known as FDTD method can be employed for two-dimensional or three-dimensional modeling of electromagnetic field [16,17]. This method is based on iterative numerical solution of Maxwell equations simulating wave propagation in sequence of very short time steps. Both small space and time steps that must be used within this method make FDTD extremely computationally demanding. Therefore only very small volumes can be analyzed using FDTD method. On the other hand, the method is very general and can incorporate any geometry, material properties and incident waves.

For the probe radiation modeling we have used the FDTD method with the following FDTD extensions:

- uni-axial perfectly matched layer (UPML) to allow waves to leave the computational domain,
- conformal modeling of the material boundaries,
- near- to far-field transform (NFFF) for evaluation of the far-field limit of the electromagnetic field distribution [18],
- computational domain stepping in one dimension to model structures elongated in one direction.

For an FDTD computation of radiation diagrams we have used these two steps:

- (1) An optical fiber probe analysis based on the geometry obtained using scanning electron microscopy and data-sheet material properties of the fiber; computed in space of $20 \times 3 \times 3$ wavelengths (λ , here 488 nm), with space discretization of $\lambda/20$, using stepping in one dimension and conformal modeling. This step was performed to validate the electromagnetic field propagation within the modeled fiber and to serve as a source for the second step.
- (2) A probe apex geometry analysis within $4 \times 4 \times 4\lambda$, space discretization $\lambda/40$, using NFFF computation of the far-field limit. The probe outer material geometry was taken from the SEM measurements and the inner geometry was varied to show the dependence of far-field radiation patterns on this parameter. The probe aperture radius was in the order of 10–30 points (within the discretization $\lambda/40$) which was a compromise between memory demands and computation precision. Far-field computation points were located at the hemisphere oriented in the same way as for the experimental measurements of far-field radiation (see Fig. 2).

As a result, we have obtained a far-field radiation distribution that could be directly compared with the experimental data measured as described in the previous section.

3. Preparation of samples and experimental arrangement

For NSOM measurements, an Aurora 2 NSOM instrument (Thermomicroscopes) was used. Standard metal shielded fiber tips (Veeco) with nominal aperture between 80 and 100 nm were used for measurements. We have used four different probes for the geometry analysis; one new probe and three probes already used in past. All the images were acquired in reflection mode; the probe was used for local sample illumination. Both shear force topography and optical data were acquired for each scan.

As a sample, we have used the standard NSOM sample (hexagonally aligned metal islands) to show the resolution capabilities of different NSOM probes.

The geometry of used NSOM probes was measured using a scanning electron microscope Jeol JSM-6460.

The experimental device used for probe radiation distribution diagram measurements consist of two goniometers driven by stepper motors and a photon counting device (PCD) from SensL company (www.sensl.com). It is able to measure the far-field radiation diagrams within a hemisphere having its center at the NSOM probe aperture (see Fig. 2). Cooled PCD is accompanied by a digital synchronous detector and chopper to measure low light intensities. As the PCD is used for the directional light intensity measurement it is sensitive enough to be used with probes with an aperture radius starting from approximately 70 nm. One goniometer can run within the range of 360° and the second one within 90° . The distance between the aperture and detector is 50 mm.

4. Results and discussion

In Fig. 1, scanning electron microscopy images of the four different NSOM probes (A–D) are presented. The ideal probe is shown in Fig. 1A. There are several defects on the probes B–D, all probably caused by a tip crash during scanning. First of all, a broken apex can be seen in Fig. 1B; this is a feature that can be observed on SEM images of NSOM probes very frequently and cannot be distinguished within NSOM measurement easily. Second, in Fig. 1C there is a probe with similar, but slightly larger defect, having some more material around the apex coming probably also from the measurement. Finally, really broken probe is presented in Fig. 1D. The probe damage at this level can be determined using video microscope installed on the NSOM or simply by looking at its total light output.

In Fig. 3, the topography and NSOM reflection images of the standard sample measured with probes B–D are presented. Probes B and C could be used for normal NSOM operation, and produced typical images of the standard sample. It can be seen that the topography images are very similar and the hexagonal structure of the aluminum islands can be easily seen on both the topography and the NSOM image. Topography measured using probe B is slightly affected by worse feedback

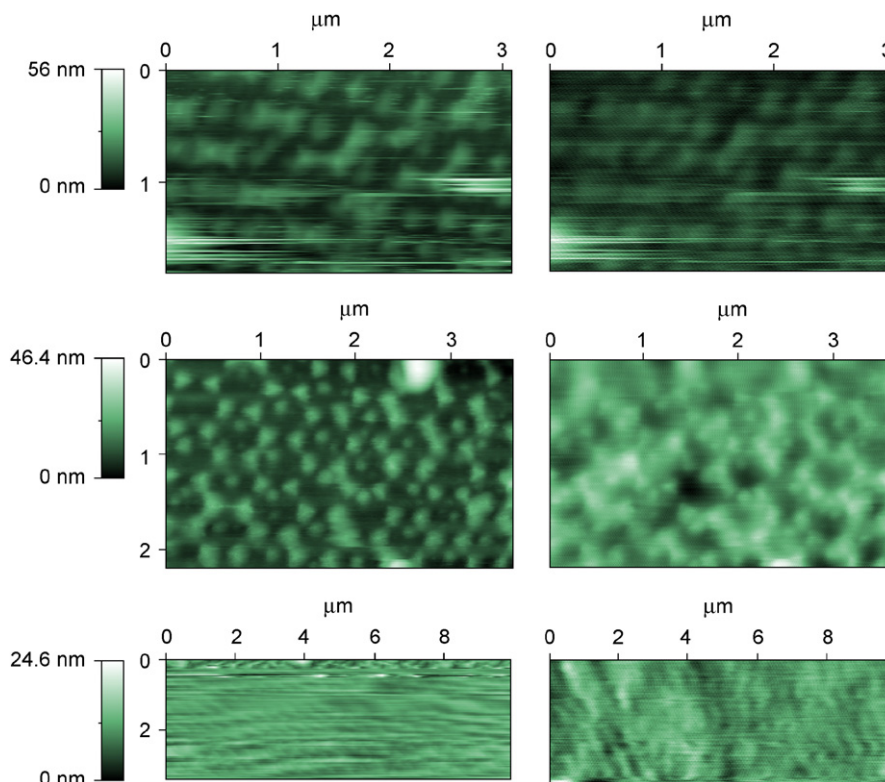


Fig. 3. Topography (left) and NSOM reflection data (right) of standard sample, measured with probes B–D.

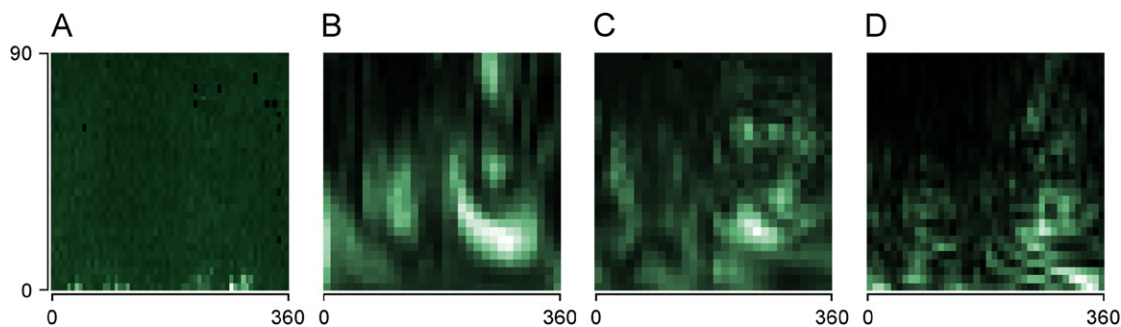


Fig. 4. Probe radiation diagrams for probes A–D.

operation (probably caused by the complicated structure of its apex). The NSOM image produced by probe B is, however, slightly better than using probe C and corresponds to a resolution of approximately 100 nm for probe B and 130 nm for probe C. Finally, the data measured using probe D are very bad, both the topography and the NSOM image. Probe D does not have the resolution abilities sufficient to measure this kind of sample.

The radiation distribution diagrams of all the probes are plotted in Fig. 4. For all the diagrams it can be seen that the mean direction of probe radiation is not optimally aligned with respect to the measuring instrument hemisphere, which is probably caused by the geometry of the tuning fork probe holder (in the ideal case, the maximum would be at the bottom horizontal line of the diagram). However, all the probes are aligned in the same way. From this and the previous figures, it can be stated that the

regularity of the radiation diagram corresponds with the probe quality. More defects on the probe apex produce more inhomogeneity in the radiation into different directions.

In Fig. 5, the one-dimensional radiation measurements are plotted for probes ‘A’ and ‘B’ to make a comparison to previous works [7]. It can be seen that for ideal, or nearly ideal probes, there is no need to measure the two-dimensional radiation diagrams. However, for heavily corrupted probes the anisotropy in the radiation directions is very large (see profiles B1 and B2) and an evaluation of probe aperture using one-dimensional scans could be problematic.

In Fig. 6, there are results of numerical simulations of probe ‘B’ far-field radiation. In Fig. 6A, the cross-section of the modeled probe geometry (base on SEM images) is presented. For the presented geometry and ideal aperture

(see Fig. 6B and E) the far-field radiation is very close to the ideal probe. However, for other aperture geometries, the results vary strongly. Note that there is a slight

difference between the simulations and measurement geometry. As the probes are not aligned ideally on the probe holder, the measured far-field radiation diagrams are sampled in different positions compared to the simulation, leading to different images. If we move and resample the measured radiation diagram to be centered at the direction of the radiation maximum (see Fig. 7) the radiation diagrams look much more similar. It can be expected that within much more computational power and more detailed sampling of the measured far-field radiation diagrams we could optimize the computational model to give the same results as observed experimentally. This will also be the topic of our forthcoming article.

5. Conclusion

It was shown that the far-field radiation diagrams can be an efficient tool for non-destructive NSOM probe analysis. With the help of the electromagnetic field modeling in the near- and far-field we can use these data for better understanding the inner probe geometry and its influence to the NSOM measurements. As the inner probe geometry

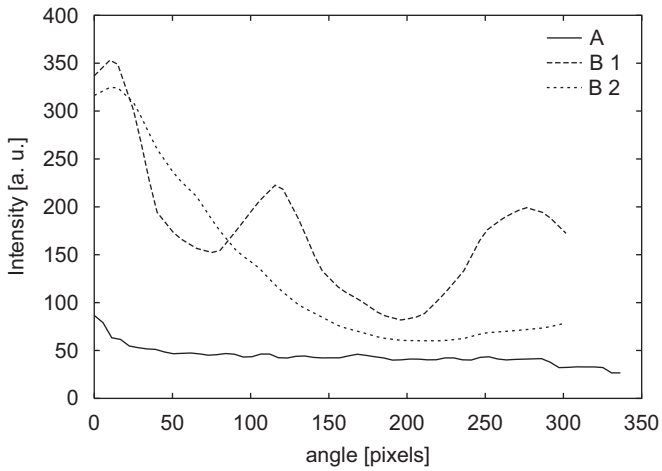


Fig. 5. One-dimensional scans for far-field radiation of probes A and B (angle scale corresponds to 0°...85°); note that probe A intensity is multiplied by a factor of 20 to be seen on the graph.

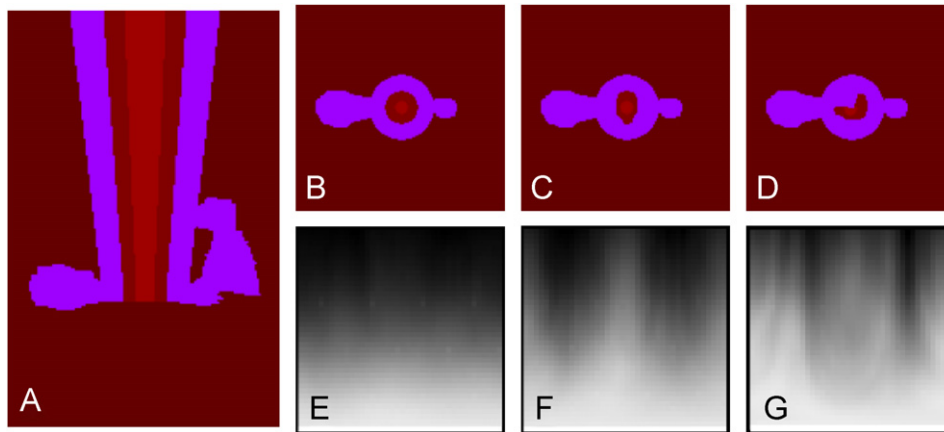


Fig. 6. Modeled probe radiation diagrams for different probe geometries. (A)—probe geometry cross-section in x-axis, (B)–(D)—probe geometry cross-sections in z-axis, (E)–(G)—corresponding far-field radiation diagrams (axis are same as in Fig. 3).

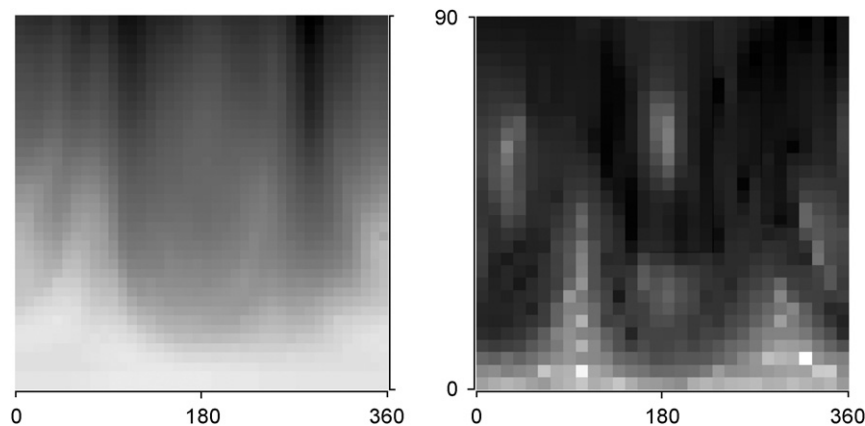


Fig. 7. Comparison of modeled probe radiation diagram (see Fig. 6G) and measured probe radiation diagram of probe B shifted to fit the maximum light output to hemisphere pole.

has deep influence on the far-field radiation diagrams, the method can be also used as a complementary tool to the SEM measurements that show only the outer geometry.

As the instrumentation for performing the probe radiation diagrams is very simple, the proposed method can be used even for daily checking of the NSOM probes between the practical measurements. The only limitation is a very small light intensity coming from probe the aperture.

References

- [1] M.A. Paesler, P.J. Moyer, *Near-Field Optics, Theory, Instrumentation and Applications*, Wiley, New York, 1996.
- [2] J.J. Greffet, R. Carminati, *Prog. Surf. Sci.* 56 (1997) 133.
- [3] B. Hecht, B. Sick, U.P. Wild, V. Deckert, R. Zenobi, O.J. Martin, D.W. Pohl, *J. Chem. Phys.* 112 (2000).
- [4] B. Hecht, H. Bielefeldt, Y. Inouye, D.W. Pohl, *J. Appl. Phys.* 81 (1997).
- [5] K.D. Weston, J.A. DeAro, S.K. Buratto, *Rev. Sci. Instrum.* 67 (1996).
- [6] O.J. Martin, Ch. Girard, A. Detreux, *J. Opt. Soc. Am. A* 13 (1996) 1801.
- [7] C. Obermüller, K. Karai, G. Kolb, G. Abstreiter, *Ultramicroscopy* 61 (1995) 171.
- [8] C. Obermüller, K. Karai, *Appl. Phys. Lett.* 67 (1995) 3408.
- [9] D. Barchiesi, Ch. Girard, O.J. Martin, D. Van Lebeke, D. Courjon, *Phys. Rev. E* 54 (1996) 4285.
- [10] J.S. Villarubia, *J. Res. Natl. Inst. Stand. Technol.* 102 (1997) 425.
- [11] T.J. Antosiewicz, T. Szoplik, *Opt. Express* 15 (2007).
- [12] O. Fenwick, G. Latini, F. Ciaciali, *Synth. Met.* 147 (2004) 171.
- [13] P.G. Gucciardi, M. Colloci, *Appl. Phys. Lett.* 79 (2001) 1543.
- [14] A. Rosenberger, A. Münnemann, F. Kiendl, G. Güntherodt, P. Rosenbusch, J.A.C. Bland, G. Eggers, P. Fumagalli, *J. Appl. Phys.* 89 (2001) 7727.
- [15] L. Alvarez, M. Xiao, *Opt. Commun.* 260 (2006) 727.
- [16] S.H. Simpson, S. Hanna, *Opt. Commun.* 256 (2005) 476.
- [17] J.T. Krug, E.J. Sanchez, X.S. Xie, *J. Chem. Phys.* 116 (2002) 10895.
- [18] O.M. Ramahi, *IEEE Trans. Antennas Propag.* 45 (1997).